Biomass Conversion and Biorefinery (2022) 12:5881–5900
https://doi.org/10.1007/s13399-020-01071-8

ORIGINAL ARTICLE

Carbon dioxide torrefaction of oil palm empty fruit bunches pellets: characterisation and optimisation by response surface methodology

Bemgba B. Nyakuma[1] · Syie L. Wong[1] · Hasan M. Faizal[2] · Hambali U. Hambali[1,3] · Olagoke Oladokun[1] · Tuan Amran T. Abdullah[1,3]

Received: 5 July 2020 / Revised: 1 October 2020 / Accepted: 9 October 2020 / Published online: 17 October 2020

Abstract

The carbon dioxide (CO_2) torrefaction of oil palm empty fruit bunch (OPEFB) pellets was investigated at various temperatures from 250 to 300 °C and residence times from 15 to 60 minutes. The objective was to investigate the effects of CO_2 torrefaction on the yield and characteristics of the torrefied products. The optimal conditions for maximum mass yield (M_Y) of CO_2 torrefaction were also examined by response surface methodology (RSM) using full factorial design. Results revealed that temperature and time significantly influenced the mass (M_Y), liquid (L_Y) and gas (G_Y) yields. The M_Y and energy yield (E_Y) decreased with increasing severity of torrefaction, whereas the L_Y, G_Y, energy density (D_E) and higher heating value (HHV) increased during the process. Characterisation revealed substantial improvements in the microstructure, pH, hydrophobicity and grindability of the torrefied pellets compared with the raw pellets. The thermal ignition and degradation characteristics of the OPEFB pellets were also significantly transformed after torrefaction. The liquid torrefaction products contained an acidic, turbid and pungent mixture of water and organic compounds. RSM optimisation revealed the optimal conditions: temperature of 275 °C and residence time of 35 minutes with the predicted M_Y of 50.54%, mass loss of M_L = 49.46% and HHV = 24.47 MJ/kg. The findings revealed that CO_2 torrefaction is a practical approach to clean energy recovery.

Keywords Carbon dioxide · Torrefaction · Oil palm · Empty fruit bunch · Pellets · Optimisation

Nomenclature

AAEM	Alkali and alkali earth metals
AC	Ash content
AIM	Agency for innovation in Malaysia
ANOVA	Analysis of variance
CO2	Carbon dioxide
CPKO	Crude palm kernel oil
CPO	Crude palm oil
D_E	Energy density
E_Y	Energy yield
FBT	Fixed bed tubular
FC	Fixed carbon
GNI	Gross national income
G_Y	Gas yield
HHV	Higher heating value
KFT	Karl Fischer titration
L_Y	Liquid yield
MC	moisture content
M_L	Mass loss (%)
M_Y	Mass yield (%)
O_2	Oxygen
OOC	Optimal operating conditions
OPEFB	Oil palm empty fruit bunch
OPEFB pellets	Oil palm empty fruit bunch pellets
OPT	Oil palm trunks
OPW	Oil palm wastes
PKS	Palm kernel shells
R_M	Residual mass (%)
RSM	Response surface methodology
SEM	Scanning electron microscope
S_F	Severity factor

✉ Bemgba B. Nyakuma
bbnyax1@gmail.com

[1] School of Chemical and Energy Engineering, Faculty of Engineering, Universiti Teknologi Malaysia, 81310 Skudai, Johor, Malaysia

[2] School of Mechanical Engineering, Faculty of Engineering, Universiti Teknologi Malaysia, 81310 Skudai, Johor, Malaysia

[3] Centre of Hydrogen Energy, Institute of Future Energy, Universiti Teknologi Malaysia, 81310 Skudai, Johor, Malaysia

t	Residence time (minutes)
TGA	Thermogravimetric analysis
T_{end}	Offset temperature (°C)
T_h	Torrefaction temperature (°C)
T_{max}	Peak decomposition (°C)
T_{mid}	Midpoint temperature (°C)
T_{ons}	Onset temperature (°C)
TPC	Temperature profile characteristics
T_r	Reference temperature (100 °C)
VM	Volatile matter

1 Introduction

The cultivation of the African oil palm tree (*Elaeis guineensis* Jacq.) for crude palm oil (CPO) and crude palm kernel oil (CPKO) production is a major socio-economic activity in Malaysia [1, 2]. Over the years, the demand for CPO and CPKO as critical raw materials for the production of bioenergy, biochemicals, biofuels and biomaterials has soared geometrically [3, 4]. Given the growing global demand, the cultivation of oil palm in Malaysia has expanded significantly from 0.64 million hectares in 1975 to 5.9 million hectares in 2018 [5]. This expansion in the acreage of oil palm cultivation has correspondingly increased CPO production to over 18 million tonnes on average yearly [5]. Consequently, Malaysia's trade in palm oil products is valued at RM$68–80 billion annually or 8% of gross national income (GNI) [6].

Conversely, the rapid expansion of the palm oil industry has created numerous challenges [7]. For example, the poor disposal and management of oil palm wastes (OPW) in palm oil mills and plantations remain a major socio-economic and environmental problem. According to the agency for innovation in Malaysia [6], the industry generates over 100 million dry tonnes of OPWs comprising oil palm empty fruit bunches (OPEFB), palm kernel shells (PKS), oil palm trunks (OPT), mesocarp fibres and fronds [8, 9]. Currently, OPWs are utilised as boiler fuel to generate heat, steam, and electricity in palm oil mills as well as organic manure, mulching additives, erosion barriers, and soil enhancers in oil palm plantations [10, 11]. Numerous studies have also highlighted the use of OPWs as renewable sources of polymers, biocomposites, and biosorbents [12, 13]. The resulting effect is that large quantities of OPWs remain strewn at plantations, open pits, dumps or landfills, thereby exacerbating land degradation and air and water pollution problems.

Over the years, the government of Malaysia enacted policies such as the Fifth Fuel Policy, Eight Malaysia Plan and the National Biomass Strategy to address the challenges currently posed by OPWs through commercial waste valorisation. The valorisation of OPW into renewable and sustainable energy, fuels and chemicals is hampered by numerous challenges. Typically, OPWs are bulky and heterogeneous and contain high moisture, ash, alkali and alkali metal contents, which result in poor grindability, low energy density and calorific values [9, 14]. The outlined challenges are predominant in OPEFB, which is the high moisture, brownish grey, spikey and bulky residue generated after the shredding and stripping of oil palm fruits from fresh fruit bunches during CPO extraction [14, 15]. Due to its high moisture content and heterogeneous nature, OPEFB is considered one of the most problematic OPWs generated during CPO production [16]. Likewise, the valorisation of OPEFB through biochemical (anaerobic digestion) and thermochemical (pyrolysis, gasification) processes is prone to low product yields, energy content, tar formation, bed agglomeration, sintering and fouling [17–19]. The poor performance of OPEFB during the high-temperature thermal conversion processes is attributed to its high moisture, ash and metal oxides composition. Hence, OPEFB requires extensive pre-treatment through pelletization and torrefaction to improve its fuel properties.

Pelletization involves the compaction of loose particles into a solid form known as pellets [20]. Typically, biomass pellets exhibit improved physicochemical, mechanical, energy content and calorific properties. Biomass pellets are also less susceptible to moisture or microbial damage, which enhances energy conversion, storage or transportation [21, 22]. Various studies have investigated the densification of OPEFB into pellets [21, 22], whereas others examined its fuel potential for pyrolysis [23], steam explosion [24] and gasification [25]. Torrefaction is the low temperature (200–350 °C) pre-treatment of biomass at short residence times (15–60 minutes) and low heating rates (5–20 °C/min) [26, 27]. During torrefaction, an inert gas such as nitrogen [28, 29] or other mildly oxidising gases or mixtures such as combustion flue gas [30, 31], oxygen (O_2) [32, 33] and carbon dioxide (CO_2) [34, 35] are used to either maintain the required process atmosphere or purge the gases evolved during the process.

Uemura et al. [28] examined the torrefaction of pulverised OPEFB from 200 to 300 °C. The process resulted in low M_Y = 43–24%, E_Y = 83–56% and HHV = 17.17–20.41 MJ/kg compared with M_Y = 77–71%, E_Y = 93–100% and HHV of 18.55–21.68 MJ/kg for palm kernel shells reported by Asadullah et al. [36]. Overall, the results showed that the pulverised OPEFB possessed lower HHV values and mass and energy yields compared with PKS. The plausible inference is that the type, nature and particle size of the biomass significantly influence the torrefaction process. Pulverised biomass particles (< 1 mm) are prone to over-oxidation and rapid internal diffusion of vapours, which are ascribed to the mildly exothermic nature of torrefaction [37]. Hence, the torrefaction of pulverised biomass results in poor product yields, HHV and thermodynamic losses [38, 39]. Given the critical need to address these challenges, Chin et al. [40] investigated the optimum conditions for the torrefaction of OPT and OPEFB through RSM. The findings revealed that

torrefaction between 250 and 300 °C resulted in M_Y (80.95–90.11%) and HHV (24.17–24.34 MJ/kg) for OPEFB, whereas OPT recorded M_Y (88.45–91.95%) and HHV (17.96–21 MJ/kg). The optimal conditions (temperature and time) for maximum HHV (24.30 MJ/kg) of torrefied OPEFB were 230 °C and 40 minutes, whereas OPT (HHV = 21.82 MJ/kg) were 300 °C and 45 minutes. Hence, optimisation through RSM is a practical technique for determining the best operating conditions for high M_Y and HHV during torrefaction.

Furthermore, the torrefaction of pelletized biomass through waste flue gases or CO_2 could potentially address the outlined challenges of pulverised biomass torrefaction under nitrogen or other inert gases, which is impractical for commercial applications. Therefore, this study seeks to critically examine the CO_2 torrefaction of OPEFB pellets using a horizontal tubular fixed bed reactor. To the best of the authors' knowledge, there are currently no studies on the torrefaction, characterisation, and optimisation of OPEFB pellets using CO_2 in the literature. The comprehensive examination of the yields, distribution and characteristics of the torrefied OPEFB pellet products was conducted. Lastly, optimization was conducted by RSM to determine the optimal conditions high M_Y from the CO_2 torrefaction of OPEFB pellets.

2 Experimental

2.1 Raw material and its properties

The OPEFB pellets were purchased from a palm oil processing mill (Felda Semenchu Sdn Bhd) situated at Kota Tinggi in Johor Darul Takzim, Malaysia, and used without further modification. Figure 1 shows the pictorial depiction of the OPEFB pellets used in this study.

The OPEFB pellets are cylindrical in shape with dimensions of 8 mm in diameter, the average length of 3 ± 1.5 cm, the mass of 2.5 g, bulk density of 800 kg/m^3 and moisture content of < 8.0 wt.%, which are similar to the values presented in the literature [41, 42]. The pellets were produced at the pressure of 60 MPa based on the piston press technology.

Fig. 1 Appearance of the OPEFB pellets

2.2 Reactor design

The torrefaction of the OPEFB pellets was performed in the horizontal fixed bed tubular (FBT) reactor depicted in Fig. 2. The set up consists of a stainless steel FBT reactor (dimensions: Length, L = 30 cm; Diameter, d = 2.54 cm) heated by an external electrical tube furnace (Lindberg Blue M, Thermo Scientific, USA). The Lindberg Blue furnace with model No TF55035A-1 is equipped with a digital, multi-segment programmable and microprocessor-based self-tuning PID control that provides optimal thermal heating during operation. The furnace is equipped with embedded heating elements that provide fast heat-up and recovery for processes in the temperature range of 100–1100 °C. During operation, the set point and actual temperatures are displayed simultaneously on the controller, which are monitored by factory fitted Platinel^{TM} II thermocouples along with self-tuning PID control to prevent overshooting of the set values and ensure the reliability and accuracy of the device. Lastly, the furnace is fitted with the Moldatherm® ceramic fibre to ensure thermal insulation and prevent heat losses.

The torrefaction setup consists of the CO_2 gas (Product gas code: MM33977 from Mega Mount Gas, Malaysia) supply unit with flow controlled by a digital flow monitor (Tylan Model: RO-32, USA). The gas and liquid torrefaction products were cooled using a chiller (Protech 631D, USA) and collected in a conical flask (V = 250 ml, Pyrex, USA). The torrefaction and setup temperatures were monitored using a type-K thermocouple and temperature data logger (Ohkura Electric Company Ltd., Japan). In this study, the selected conditions for the CO_2 torrefaction of the OPEFB pellets were temperature (T) of 250, 275, and 300 °C; residence time (t) of 15, 30 and 60 minutes at 1 atm, 15 °C/min; and gas flow rate of 200 mL/min. Based on these conditions, the design of experiments (DoE) for the torrefaction of OPEFB pellets under CO_2 gas conditions was performed in the study.

2.3 Experimental procedure

The experimental procedure for the CO_2 torrefaction of the OPEFB pellets is presented in this section of the paper. For each experiment, 15 g of OPEFB pellets was loaded into the FBT, which was then placed in the tubular electrical furnace before purging with CO_2 for 15 minutes at 200 mL/min. The reliability and accuracy of the purge gas flow rate were verified visually using a digital flow monitor. After flushing was completed, the FBT reactor and OPEFB pellets were heated under non-isothermal (dynamic) conditions by ramping from

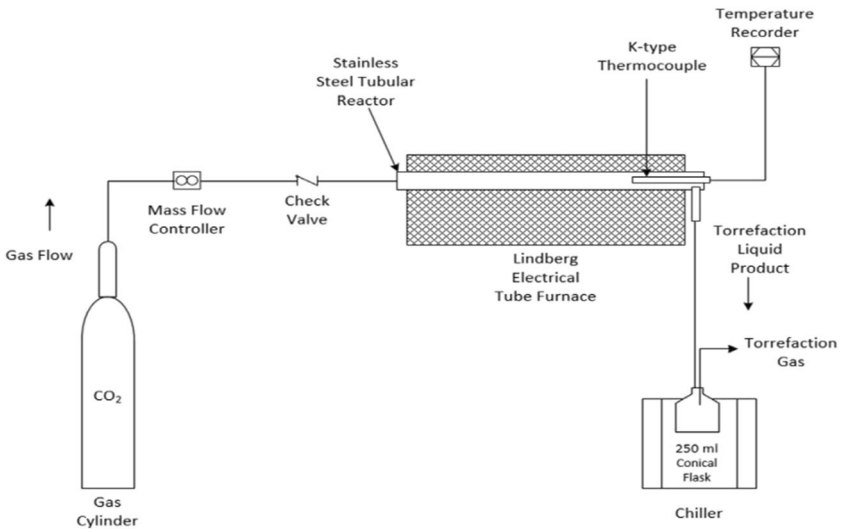

Fig. 2 Schematic of the FBT reactor for OPEFB pellet torrefaction

room temperature to the selected torrefaction temperature (T = 250, 275 or 300 °C) at a constant heating rate of 15 °C/min. At the selected torrefaction temperature, the isothermal mode was activated, and heating was maintained at the residence times (*t* = 15, 30 or 60 minutes). On completion, the furnace was switched off and the FBT reactor was cooled down to ambient temperature. Next, the torrefied OPEFB pellets were retrieved, weighed, and stored in airtight vessels before characterisation. Likewise, the liquid torrefaction products were collected in the conical flask, weighed, and stored in airtight sample bottles before refrigeration at 5 °C before characterisation.

The gas product was flared off during torrefaction. Each test was performed in duplicate, and the final results presented as average values. The performance of the CO_2 torrefaction process was examined based on the M_Y, E_Y, D_E and S_F computed as follows:

$$M_Y = \left(\frac{m_{TB}}{m_{RB}}\right) \times 100 \tag{1}$$

$$E_Y = M_Y \times \left(\frac{HHV_{TB}}{HHV_{RB}}\right) \tag{2}$$

$$D_E = \left(\frac{E_Y}{M_Y}\right) \tag{3}$$

$$S_F = log\left\{t \times exp\left(\frac{T_h - T_r}{14.75}\right)\right\} \tag{4}$$

The term m_{TB} is defined as the mass of the torrefied biomass (g), m_{RB} the mass of the raw biomass (g), M_Y the mass yield (%), E_Y the energy yield (%), D_E the energy density, HHV the higher heating value (MJ/kg) and S_F the severity factor. The S_F terms t, T_h and T_r are the torrefaction residence time (minutes), temperature (°C) and reference temperature (100 °C), respectively.

2.4 Optimization procedure

The optimization of the CO_2 torrefaction of OPEFB pellets was performed by response surface methodology (RSM) using Statistica (StatSoft Enterprise Software, version 8.0). In this study, the two-factor three-level (3^2) full factorial design was employed to analyse the effects of the independent variables: temperature (X_1 = 250–300 °C) and time (X_2 = 15–60 mins) on the CO_2 torrefaction of the OPEFB pellets. The selected design of experiments

Table 1 DoE for CO_2 Torrefaction of OPEFB pellets

Run number	Replicates	Temperature (X_1, °C)	Time (X_2, minutes)
5	R1	275	30
17	R2	300	30
4	R1	275	15
6	R1	275	60
1	R1	250	15
12	R2	250	60
10	R2	250	15
7	R1	300	15
2	R1	250	30
18	R2	300	60
16	R2	300	15
8	R1	300	30
14	R2	275	30
9	R1	300	60
15	R2	275	60
11	R2	250	30
13	R2	275	15
3	R1	250	60

(DoE) included 1 block and 1 replicate comprising a total of 18 runs, as summarised in Table 1.

The experimental runs in Table 1 were conducted randomly to minimize the influence of inexplicable variances due to disparate variables. The selected design was based on its successful application in the optimization of biomass torrefaction reported in the literature [40, 43]. The selected independent variables were temperature (X_1) and time (X_2), whereas the dependent variable (response) was the M_Y of the OPEFB pellets after CO_2 torrefaction.

Therefore, the mathematical model correlating the independent and dependent variables to the selected response was deduced from the built-in analysis function of Statistica. Consequently, the model for the 3^2 full factorial design used in this study was deduced as

$$Y = \beta_0 + \beta_1 X_1 + \beta_2 X_2 + \beta_n X_n \quad (5)$$

The term Y represents the predicted response; β_o the intercept coefficient (offset); β_1, β_2 and β_n are the linear or first-order terms; and lastly, X_1, X_2 and X_n are the independent variables. Based on Eq. (5), the operating conditions for CO_2 torrefaction were optimized based on the 3^2 full factorial design. Next, the accuracy and validity of optimization were examined by analysis of variance (ANOVA) to deduce the validity, residual and regression coefficients of the process variables. The optimal operating conditions (OOC) for the OPEFB pellets CO_2 torrefaction process were determined through multi-response desirability profiling in Statistica. The multi-response desirability profiler was aggregated to maximize the predicted response model (Y) based on the overall mean values of M_Y determined from ANOVA. The predicted results were then computed and plotted to deduce the OOC. The RSM optimization results were validated by performing confirmatory experiments at the OOC. Lastly, the results were compared with the predicted values to determine the consistency of the optimization process.

2.5 Products, yield and distribution

The product yields of biomass torrefaction are typically solid, liquid, and gases [27], which are denoted as M_Y, L_Y, and G_Y, respectively. The product distribution of torrefaction was computed from Equations 6, 7, and 8, respectively.

$$L_Y, \% = \frac{m_{mass\ of\ liquid\ in\ conical\ flask}}{m_{Raw\ Biomass}} \times 100 \quad (6)$$

$$G_Y, \% = 100 - (M_Y + L_Y) \quad (7)$$

$$M_Y + L_Y + G_Y = 100\% \quad (8)$$

2.6 Liquid torrefaction characterisation

The liquid products of the CO_2 torrefaction process were characterised to determine the pH, colour as well as the water/organics composition to examine its potential impacts on the environmental or future applications.

2.6.1 Colour and composition analysis

After the CO_2 torrefaction process, the liquid torrefaction products were collected and stored in 30-ml glass vial sample bottles. The colour and composition of the L_Y products were then examined by visual and photographic analysis to examine the effects of the reaction parameters on the CO_2 torrefaction process.

2.6.2 pH analysis

The pH analysis of the liquid torrefaction product was analysed using the benchtop pH metre (Martini Instruments M*i* 150, USA). For each test, the liquid torrefaction products were transferred from the sample bottles into 100 ml beakers (Pyrex, USA). Subsequently, the pH electrode was immersed in the beaker containing the liquid to obtain the pH meter readings which were recorded every 10 seconds to determine the pH of each sample.

2.6.3 Water and organics analysis

The water and organics contents of the liquid torrefaction products were determined by Karl Fischer Titration (KFT) using the Karl Fischer titrator (Metrohm AG, 870 KF Titrino plus, Switzerland). The titrator was equipped with twin systems for dosing (Metrohm AG 800 Dosino, Switzerland) and mixing (Metrohm AG 803 Ti Stand, Switzerland). The selected reagent for the KFT analysis was Hydranal purchased from Fluka Analytical (Sigma-Aldrich, Malaysia), whereas the Tiamo™ software (version 1.2) was used for data collection and analysis. Before each test, the KF titrator was standardised with distilled water to verify the consistency of the experiments. The setup for the starting drift was 2.4 μL/min based on a 10-second delay after obtaining the conditioning OK signal. For each test, about 0.09 g of each sample was measured in a 10-μL syringe (Hamilton, Switzerland) before addition to the mixing chamber that contained the Hydranal reagent to begin the process of titration. At the endpoint of the titration, the titre readings were recorded, and the titration vessel was emptied into the waste collection bottle. Next, the water and organics contents were computed in Eqs. 9 and 10:

$$Water\ Content\ (\%) = \left(\frac{KFR_{Consumed} \times KFR_{Factor}}{W_{Sample}}\right) \times 100 \quad (9)$$

$$Organics\ Content\ (\%) = 100 - Water\ Content\ (\%) \quad (10)$$

The terms $KFR_{consumed}$, KFR_{Factor} and W_{sample} are the volume of Karl Fischer Reagent consumed (ml) during titration, reagent factor (mg/ml) and mass of sample (g), respectively.

2.7 Solid torrefaction product material properties

The raw and torrefied OPEFB pellets were characterised to determine their physicochemical, thermal, microstructure, mineralogical, pH, grindability, hydrophobicity and thermal properties.

2.7.1 Physicochemical analyses

The physicochemical fuel properties of the raw and torrefied OPEFB pellets were characterised by ultimate, proximate and calorific analyses. The ultimate analysis was performed through an elemental analyser (vario MACRO Cube, Germany) to compute the composition of carbon (C), hydrogen (H), nitrogen (N) and sulphur (S) based on ASTM D5291 standard. The oxygen (O) composition was determined by difference from the sum of the percentage of the CHNS elements. Proximate analysis was performed in a muffle furnace (Ney Vulcan D-130, USA) according to ASTM D3173 for moisture (MC), D3174 for ash (AC) and D3175 for volatile matter (VM). Fixed carbon (FC) was determined by difference from the sum of MC, AC and VM. The calorific value of the raw and torrefied OPEFB pellets was measured using an oxygen bomb calorimeter (IKA C2000, USA). All tests were repeated to confirm the reliability of the measurements.

2.7.2 Microstructural analyses

The microstructural compositions of the raw and torrefied OPEFB pellets were investigated by scanning electron microscopy (SEM) (JEOL JSM IT-300 LV, Japan). Before each test, the samples were pulverised in a dry miller (Panasonic MX-AC400, Malaysia) and sifted through an analytical laboratory sieve (W.S. Tyler Mesh Size No. 60, USA). Next, the powdered samples were spray-coated on prepared grain mounts, transported and degassed in the SEM sample compartment to purge off extraneous materials. The samples were subsequently scanned to obtain surface micrographs in vacuum at a magnification of ×1000 using the point ID technique.

2.7.3 pH analysis

The pH analysis of the raw and torrefied OPEFB pellets was examined based on the Rajkovich et al. [44] procedure. Precisely 0.5 g of each pulverised sample was mixed with 10 ml of distilled water based on the ratio of 1:20. Each mixture was placed in a 250 ml beaker (Pyrex, USA) before transferring to a magnetic stirrer (Jenway 1103, USA), and twirled vigorously for 1.5 hours at 300 rpm. Next, the mixtures were filtered using filter papers (Smith A0331, 101 Qualitative 125 mm, United Kingdom). The pH of the filtrate was then analysed using the benchtop pH meter (Martini Instruments M*i* 150, USA). Before each test, the pH meter was recalibrated and the pH electrode cleaned with distilled water to ensure the consistency of the measurements. Next, the pH electrode was gently dipped into the filtrate to determine its pH based on multiple measurements recorded every 10 seconds.

2.7.4 Hydrophobicity analysis

The hydrophobic properties of the raw and torrefied OPEFB pellets were investigated according to the procedure by Pimchuai et al. [45]. Before each run, the raw and torrefied OPEFB pellets were first weighed and transferred into 100-ml ceramic crucibles. Next, distilled water (20 ml) was added, and the mixture was stowed away for 2 hours. On completion, the samples were retrieved and weighed to determine the percentage of water absorbed based on the relation [45]:

$$Water\ Absorbed, \% = \left(\frac{m_{H2O\ absorbed}}{m_{Sample}}\right) \times 100 \quad (11)$$

where the symbols $m_{H2O,\ absorbed}$ and m_{sample} denote the mass of water absorbed (g) and mass of the torrefied OPEFB pellets (g).

2.7.5 Grindability analysis

The hardgrove grindability index (HGI) described by Ibrahim et al. [46] was employed to examine the grindability of the raw and torrefied OPEFB pellets. Before the test, each pellet was pulverised in the dry miller (Panasonic MX-AC400, Malaysia) for 1 minute. Next, a fixed mass (1 ± 0.1 g) of each pulverised sample was sieved by agitation using in the 74-micron sieve (W.S. Tyler Mesh Size No. 200, USA) for 2 minutes at room temperature. On completion, the percentage mass of each sample that permeated the sieve was weighed and recorded as m_H to compute the HGI as follows:

$$HGI = \frac{m_H + 11.205}{0.4955} \quad (12)$$

The term m_H is the percentage mass of each sample that exited the 74-micron sieve. Typically, the lower the HGI value, the harder it is to grind the sample [47]. Lastly, the grindability scales of Ohliger et al. [48] were employed to evaluate the HGI of the raw and torrefied OPEFB pellets.

2.7.6 Thermal analysis

The thermal degradation and temperature profile characteristics of the raw and torrefied OPEFB pellets were examined through thermogravimetric analysis (TGA). For each test, 10 mg of each pulverised sample was placed in an alumina crucible and heated in the TGA (Shimadzu TG-50, Japan). The heating rate of 20 °C/min and a non-isothermal program was used to heat the samples from 30–800 °C using air as purge gas and to simulate oxidative (combustion) thermal degradation. On completion, the TGA data was recovered from the Shimadzu thermal analysis workstation (version: TA-60WS) software to determine the mass loss (M_L) and temperature profile characteristics (TPC) of each sample. Next, the mass loss (%) and derivative of mass loss (%) data were plotted against temperature (°C) in Microsoft Excel© (version 2013) to obtain the thermogravimetric (TG, %) and derivative thermogravimetric (DTG, %/min) plots, respectively. Based on the plots, the TPCs, onset (T_{ons}), midpoint (T_{mid}), peak decomposition (T_{max}), offset (T_{end}) temperatures and residual mass (R_M) were deduced to examine the thermal degradation behaviour of each sample.

3 Results and discussion

3.1 Product yield and distribution

Figures 3, 4 and 5 depict the effects of the independent variables (X_1 and X_2) on the M_Y, L_Y and G_Y for the CO_2 torrefaction of OPEFB pellets. For the CO_2 torrefaction process at the residence time of 15 minutes, the L_Y increased from 10.20 to 34.31% and G_Y increased from 5.38 to 23.14%, whereas the M_Y decreased (84.42 to 42.54%) with increasing temperatures. For the 30-minute CO_2 torrefaction process, the L_Y increased from 19.26 to 37.81% and G_Y increased from 14.91 to 21.81%, whereas the M_Y decreased from 65.84 to 40.38%. Similarly, an incremental trend was observed for L_Y and G_Y, whereas the M_Y decreased with increasing severity during the 60-minute torrefaction process. It can be reasonably inferred that for all cases, the values of L_Y and G_Y increased, whereas M_Y decreased with increasing severity of the torrefaction temperatures and residence times. Furthermore, the temperature variations influenced M_Y more significantly than L_Y and G_Y as observed in the 15- and 30-minute process.

The plausible inference is that at higher temperatures, the rate of thermal degradation of the lignocellulosic components and devolatilization of organic matter was greatly enhanced during the CO_2 torrefaction process. Hence, the OPEFB pellets were thermally degraded into solid char along with condensable and non-condensable gaseous products. Over time, the condensable gas fractions were subjected to secondary cracking, and the products subsequently condensed into the liquid products resulting in the higher L_Y values, as observed during the 30- and 60-minute torrefaction runs.

The CO_2 torrefaction process was further examined through energy yield (E_Y), energy density (D_E), higher heating value (HHV) and severity factor (S_F) as presented in Table 2.

The results indicate that the D_E, HHV and S_F were improved with increasing temperatures and residence times during the CO_2 torrefaction process. However, E_Y exhibited a decreasing trend, which can be attributed to the declining M_Y during the process. As observed, the E_Y decreased from 102.37 to 54.05, whereas D_E increased from 1.21 to 1.47 due to the increase in HHV from 21.31 MJ/kg to 25.74 MJ/kg over the entire range of conditions examined in this study. Therefore, a significant improvement in the HHV was observed compared with the HHV of 17.57 MJ/kg for the raw OPEFB pellets. Lastly, the S_F was improved from 5.59 to 7.67 after torrefaction.

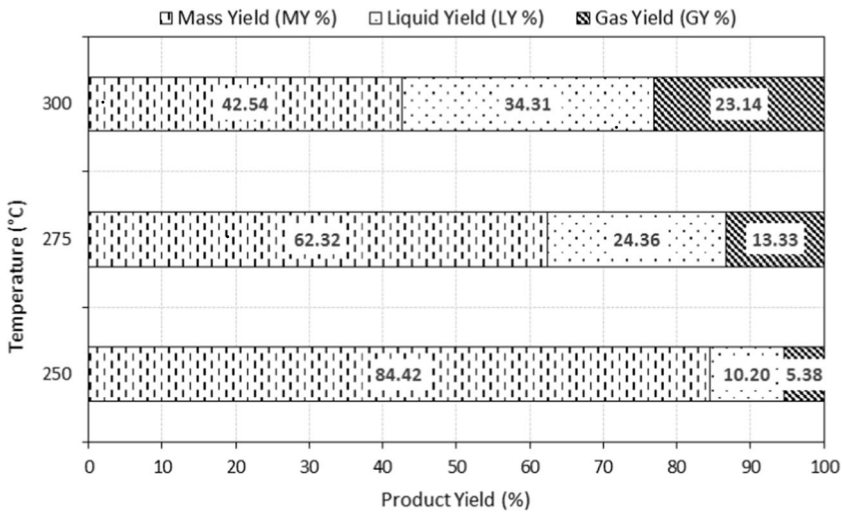

Fig. 3 Product yield of CO_2 torrefaction for 15 minutes

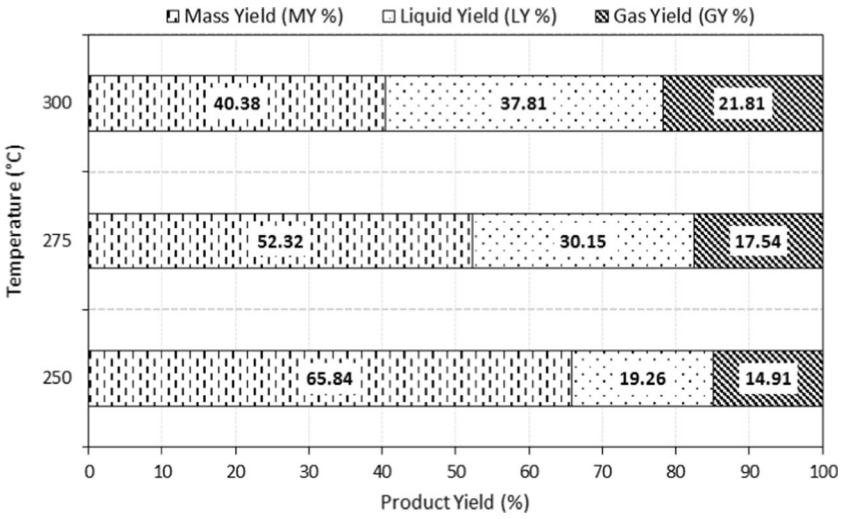

Fig. 4 Product yields of CO_2 torrefaction for 30 minutes

In general, the increase in temperatures (250–300 °C) and residence times (15–30 mins) showed marked improvements in torrefaction parameters (E_Y, D_E, HHV and S_F) for the OPEFB pellets. However, further analysis showed that the increase in residence time from 30 to 60 mins resulted in only negligible improvements of D_E (0.70%), HHV (0.53%) and S_F (4.56%) on average for all temperatures. In contrast, the E_Y decreased from 0.54% (250 °C) to 7.48% (300 °C) with increasing residence time from 30 to 60 mins. Therefore, the 30-min process for the CO_2 torrefaction of OPEFB pellets is sufficient for enhanced performance and product yield. Similar findings have been reported in the literature [26, 45].

3.2 Liquid torrefaction properties

The properties of the liquid products produced from the CO_2 torrefaction process were examined in terms of colour composition, pH, and water content.

3.2.1 Colour and composition

The CO_2 torrefaction of the OPEFB pellets from 250 to 300 °C for 30 mins yielded 19.26–37.81% of liquid products, respectively. The liquid products were collected in 30-ml glass vial sample bottles prior to analysis, as depicted in Fig. 6.

As observed, the colours of liquid products were transformed from light brown (at 250 °C) to dark brown (at 275 °C) and black (at 300 °C). Hence, the increase in severity of torrefaction affected not only the colour of the products but also the release of more pungent odours. The strong odours could be attributed to the aromatic, aldehyde, ester, organic acid and volatile compounds [49] generated by the thermally catalysed aromatization and degradation of holocellulose and lignin during torrefaction [50, 51]. Further analysis revealed that the liquid products generated at 275 °C and 300 °C each contains two-phase layers (Fig. 6(b) and (c)). Consequently, the pH and composition of the 2-phase layer were examined by pH analysis and Karl Fischer Titration (KFT), respectively.

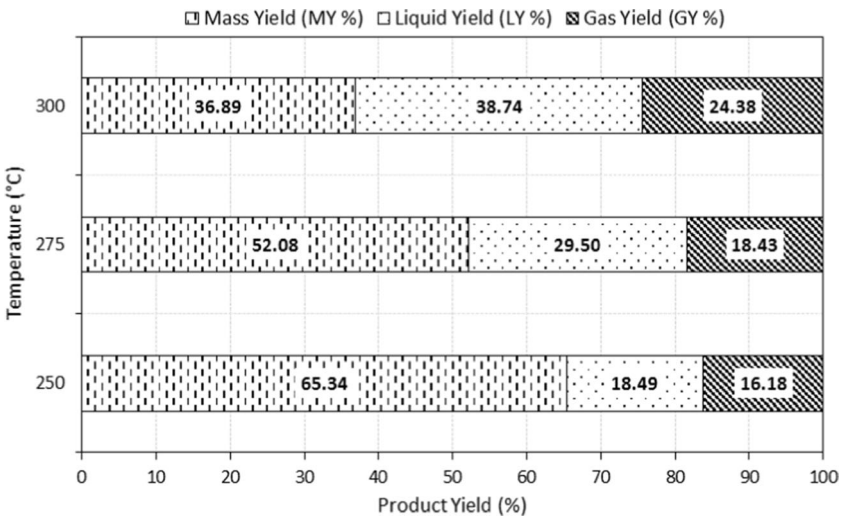

Fig. 5 Product yields of CO_2 torrefaction for 60 minutes

Table 2 Performance of the CO_2 torrefied OPEFB pellets

Sample/ torrefaction temperature (°C)	Hold time (minutes)	Energy yield (E_Y)	Energy density (D_E)	Heating value (MJ/kg)	Severity factor (S_F)
Raw OPEFB pellets	**	**	**	17.57	**
250	15	102.37	1.21	21.31	5.59
275		82.88	1.33	23.37	6.33
300		61.06	1.44	25.22	7.06
250	30	86.33	1.31	23.04	5.89
275		72.36	1.38	24.30	6.63
300		58.42	1.45	25.42	7.37
250	60	85.86	1.31	23.09	6.19
275		72.10	1.39	24.33	6.93
300		54.05	1.47	25.74	7.67

**No data available as the parameters cannot be determined for the raw OPEFB pellets

3.2.2 pH of torrefaction liquid

The analysis showed that the pH increased from 2.87 (for torrefaction at 250 °C) to 2.94 (at 275 °C) and finally to 3.13 (at 300 °C). The decrease in acidity could be ascribed to the organic matter and chemical compounds such as organic, carboxylic or aromatic acids released into the liquid [52, 53], which increased with increasing severity of torrefaction [52, 53]. Chen et al. [49] reported pH ranging from 2.27 to 2.60 for bamboo torrefaction liquid products.

3.2.3 Water and organics content

The composition of liquid products of CO_2 torrefaction of OPEFB pellets from 250 °C to 300 °C for 30 minutes was examined through KFT. The results indicate that the liquid products of the torrefaction broadly consist of water and organic fractions. The water content decreased from 65.17% (at 250 °C), 63.76% (at 275 °C) to 62.53% (at 300 °C), whereas the organic content increased from 34.83% (at 250 °C), 36.24% (at 275 °C) to 37.47% (at 300 °C). The decrease in water content can be explained by the higher drying rates at the elevated torrefaction temperatures. The conditions also resulted in higher rates for the degradation of lignocellulosic components, which explains the increase in the organic fraction after torrefaction. Overall, the increase in organic content may also account for the increase in pH from 2.87 to 3.13 (or decreasing acidity) of the liquid products.

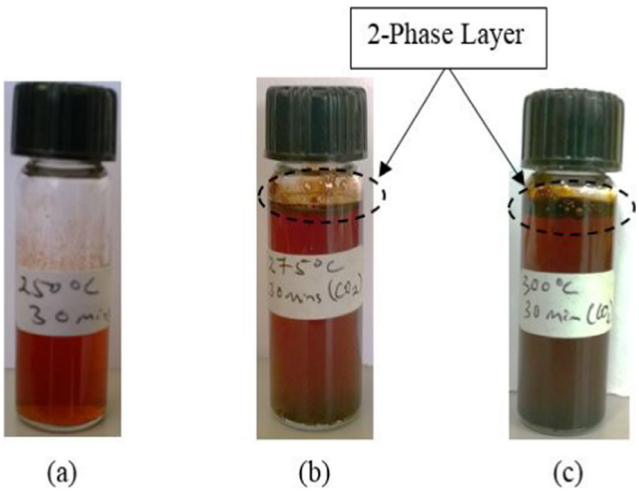

Fig. 6 Colours of liquid products from CO_2 torrefaction

3.3 Solid torrefaction product material properties

3.3.1 Physicochemical properties

Table 3 presents the physicochemical properties of the raw and CO_2 torrefied OPEFB pellets in terms of the ultimate and proximate analyses. The symbols are defined as C, carbon; H, hydrogen; N, nitrogen; S, sulphur and O, oxygen. The most significant changes in the elemental composition of the torrefied pellets were observed for C, H, and O when compared with the raw OPEFB pellets. As observed in Table 3, the elemental composition of C increased, whereas H and O decreased accordingly after torrefaction. The highest C but lowest H and O were observed for the torrefied OPEFB pellets at 300 °C and 30 mins, whereas torrefaction at 250 °C and 15 mins resulted in the lowest C but the highest H and O.

The changes in the elemental composition of C can be ascribed to the decomposition of the lignocellulosic (hemicellulose and cellulose) components and volatile matter into char [27]. However, the variations in H and O are due to drying, decarboxylation, and devolatilization [37] resulting in the loss of H_2O, CO_2, and VM [34] during the CO_2 torrefaction process. Similarly, the percentage elemental composition of N and S in the torrefied pellets also changed with increasing severity of torrefaction. In this case, the decline could be ascribed to thermally enhanced denitrification and desulfurization reactions during torrefaction. The probable explanation could be the conversion of N into NO_x and S into SO_x, which were subsequently released along with other non-condensable gaseous products during torrefaction. This view is corroborated by Kim et al. [54] who reported that the lower values of N and S observed in their study were due to thermal conversion and release along with other gaseous or liquid products of torrefaction. The findings of Kim et al. [54] and those reported in this study indicate the N and S were oxidised by O into NO_x and SO_x during torrefaction. The atomic ratios of elements for the torrefied pellets after CO_2 torrefaction were examined.

Table 4 presents the changes in the elemental or atomic ratios: H/C, O/C, C/N and CH/NS for the torrefied OPEFB pellets. For all cases, the atomic H/C and O/C ratios decreased

Table 3 Ultimate analyses of raw and CO_2 torrefied OPEFB pellets

Torrefaction temperature (°C)	Time (mins)	C (wt.%)	H (wt.%)	N (wt.%)	S (wt.%)	O (wt.%)
OPEFB pellets	**	41.71 ± 0.08	5.53 ± 0.41	1.12 ± 0.05	0.12 ± 0.01	51.53 ± 0.27
250	15	45.65 ± 0.16	5.59 ± 0.00	1.02 ± 0.02	0.20 ± 0.13	47.55 ± 0.31
275		53.54 ± 0.06	5.18 ± 0.04	0.91 ± 0.01	0.06 ± 0.00	40.29 ± 0.11
300		61.91 ± 0.04	4.62 ± 0.02	1.05 ± 0.01	0.06 ± 0.00	32.36 ± 0.03
250	30	51.41 ± 0.01	5.38 ± 0.07	0.85 ± 0.02	0.08 ± 0.01	42.28 ± 0.05
275		56.31 ± 0.15	5.04 ± 0.06	0.97 ± 0.02	0.07 ± 0.00	37.60 ± 0.07
300		62.96 ± 0.21	4.43 ± 0.04	1.05 ± 0.01	0.07 ± 0.00	31.49 ± 0.17
250	60	52.01 ± 0.03	5.33 ± 0.05	0.82 ± 0.01	0.07 ± 0.00	41.77 ± 0.06
275		58.16 ± 0.05	4.87 ± 0.04	1.05 ± 0.00	0.08 ± 0.00	35.85 ± 0.08
300		61.88 ± 0.03	4.50 ± 0.06	1.10 ± 0.03	0.07 ± 0.02	32.46 ± 0.02

with increasing severity of torrefaction. The H/C ratio decreased from 0.13 in the raw OPEFB pellets to the range 0.07–0.12, with the minimum value observed at 300 °C and 30 minutes. Similarly, the O/C ratio decreased from 1.24 in the raw OPEFB pellets to the range of 0.50–1.04, with the minimum value similarly observed at 300 °C and 30 minutes. It can be inferred that torrefaction exerted more significant effects on the H/C and O/C ratios during the 30-minute process. The C/N and CH/NS ratios increased with increasing severity of torrefaction.

The decreasing trends observed for the H/C and O/C ratios and increasing trends observed for the C/N and CH/NS ratios are due to drying, devolatilization, and decarboxylation reactions that occur during torrefaction [26, 37]. Likewise, these reactions affected the proximate properties (MC, VM, AC and FC) of the CO_2 torrefied OPEFB pellets, as similarly observed in the literature [21, 39]. The proximate analysis of the CO_2 torrefied OPEFB pellets was limited to the 30-minute process since as reported earlier, the effects of the torrefaction parameters were more evident at these conditions. Table 5 presents the proximate analyses of the OPEFB pellets torrefied from 250 °C to 300 °C for 30 minutes under CO_2.

The results show that the percentage composition of MC and VM decreased after torrefaction, whereas the AC and FC increased with increasing severity of the process conditions. The MC decreased from 7.78 wt.% in the raw OPEFB pellets to 4.32 wt.% after torrefaction at 250 °C and 1.00 wt.% at 300 °C during the 30-minute process. Similarly, the VM decreased from 75.19 wt.% for the raw OPEFB pellets to between 38.38 and 63.21 wt.% due to loss of moisture (drying) and volatiles (devolatilization) [26, 31]. Conversely, the FC increased from 11.24 wt.% in the raw OPEFB pellets to the range 23.90–34.40 wt.% after torrefaction. The marked increase in FC is also attributed to the significant loss of volatile matter during torrefaction. Typically, the FC increases with decreasing VM and serves as an important determinant of the feedstock suitability, process performance, and product yield during gasification [27].

Likewise, the percentage composition of AC increased from 5.80 wt.% in the raw OPEFB pellets to 7.62–26.21 wt.% after torrefaction between 250 and 300 °C, respectively.

Table 4 Atomic ratios of raw and CO_2 torrefied OPEFB pellets

Sample/torrefaction temperature (°C)	Time (mins)	H/C	O/C	C/N	(CH/NS)
OPEFB pellets	**	0.133	1.24	37.41	38.38
250	15	0.123	1.04	44.84	42.22
275		0.097	0.75	58.62	60.14
300		0.075	0.52	59.11	60.11
250	30	0.105	0.82	60.58	61.30
275		0.090	0.67	57.91	58.75
300		0.070	0.50	59.82	59.88
250	60	0.102	0.80	63.36	64.70
275		0.084	0.62	55.64	56.10
300		0.073	0.52	56.21	56.79

Table 5 Proximate analyses of CO_2 torrefied OPEFB pellets

Sample/torrefaction temperature (°C)	MC (wt.%)	VM (wt.%)	AC (wt.%)	FC (wt.%)
OPEFB Pellets	7.78 ± 0.13	75.19 ± 0.04	5.80 ± 0.04	11.24 ± 0.13
250	4.32 ± 0.14	63.21 ± 0.39	7.62 ± 0.07	24.85 ± 0.23
275	2.34 ± 0.16	48.91 ± 0.23	24.84 ± 0.17	23.90 ± 0.10
300	1.00 ± 0.23	38.38 ± 0.69	26.21 ± 1.47	34.40 ± 0.01

This marks a significant increase in ash, as similarly reported in the literature [34, 55]. The high ash content is due to several reasons. Firstly, the thermal degradation of hemicellulose, cellulose, and lignin during torrefaction is considered a mildly exothermic process [34, 37]. This observation suggests that partial oxidation (combustion) reactions, which typically result in ash formation, may explain the significant ash observed during CO_2 torrefaction in this study. Secondly, the high ash content could be related to the high alkali and alkali earth metals (AAEMs) content, typically reported in OPEFB [18, 56]. The AAEMs reportedly catalyse oxidative reactions during biomass gasification and pyrolysis [57, 58], which may account for the high ash observed in this study.

3.3.2 Microstructural properties

Figure 7(a–d) presents the SEM micrographs (magnification ×1000) for the raw and torrefied OPEFB pellets torrefied at 250, 275 and 300 °C for 30 minutes. The SEM micrograph of the raw OPEFB pellets (Fig. 7(a)) shows an unevenly shaped particle with a surface morphology characterised by a network of thick fibrous materials, which can be ascribed to the holocellulose and lignin components of biomass [59, 60]. The SEM micrograph of the CO_2 torrefied OPEFB at 250 °C revealed a network of dispersed fibres surrounded by groups of micropores on the sample surface. This marks the onset of defibration and compaction of the irregular shaped and elongated fibres of the raw OPEFB pellets. Typically, hemicellulose starts to thermally degrade from 220 °C to 315 °C [34], which explains why it is the most reactive and the first lignocellulose to degrade during torrefaction [37]. The observations in Fig. 7(b) are due to hemicellulose degradation during torrefaction, which has major effects on the grindability of torrefied biomass [48, 59].

In contrast, the SEM micrograph for the CO_2 torrefied OPEFB pellet at 275 °C and 30 minutes was characterised by a layer of parallel fibres or microfibrils. The structural features of the microfibrils are similar to the linear (ordered) polymeric, regularly shaped structures of cellulose [59, 61]. This observation indicates the irregular (amorphous) fibres of hemicellulose were considerably degraded (and partially cellulose) after torrefaction at 275 °C. Hence, the micropores of the raw pellets were transformed into macro-pores as evident in the crevices or channels observed in the lower-left corner of Fig. 7(c). The SEM micrograph suggests that the process ruptured the microstructure and cell wall, which could significantly improve porosity and grindability properties after torrefaction. This view is corroborated by Thanapal et al. [34] who showed that CO_2 torrefaction results in a significant pore formation and high surface area due to the partial reaction of CO_2 with biomass components. As a result, the rates of devolatilization and mass loss are enhanced due to the CO_2 torrefaction process.

Lastly, Fig. 7(d) shows the SEM micrograph of the torrefied OPEFB pellets at 300 °C and 30 mins. As observed, the OPEFB pellets experienced significant transformation, as evidenced by the heterogeneous mixture of layered and knaggy fibres that surround the numerous dispersed meso- and macroporosity of crevices. The formation of crevices observed in the micrograph akin to tracheids and vessels is mainly due to the holocellulose and lignin degradation during torrefaction. Consequently, the structural pore openings observed in the micrograph indicate significant microstructural, morphological and physicochemical transformations occurred in torrefaction.

3.3.3 pH of raw and CO_2 torrefied pellets

The pH of the torrefied OPEFB pellets is critical for non-energy applications particularly biochar used for soil amendment. The pH of the OPEFB pellets torrefied at 250, 275 and 300 °C for 30 minutes are 6.88, 7.44 and 8.20, respectively, compared with the pH of 6.65 for the raw OPEFB pellets. The findings demonstrate that CO_2 torrefaction transformed the pH of the raw OPEFB pellets from weakly acidic (pH = 6.88 at 250 °C) to moderately alkaline (pH = 8.20 at 300 °C). The authors also observed that the pH of OPEFB-derived biochar was similarly transformed from acidic to alkaline with increasing severity of torrefaction. The alkaline pH of the torrefied OPEFB pellets could be due to the high C, FC and AAEMs contained in ash residues, as reported earlier. In general, the findings indicate the CO_2 torrefied pellets could be potentially utilised as biochar for agricultural applications.

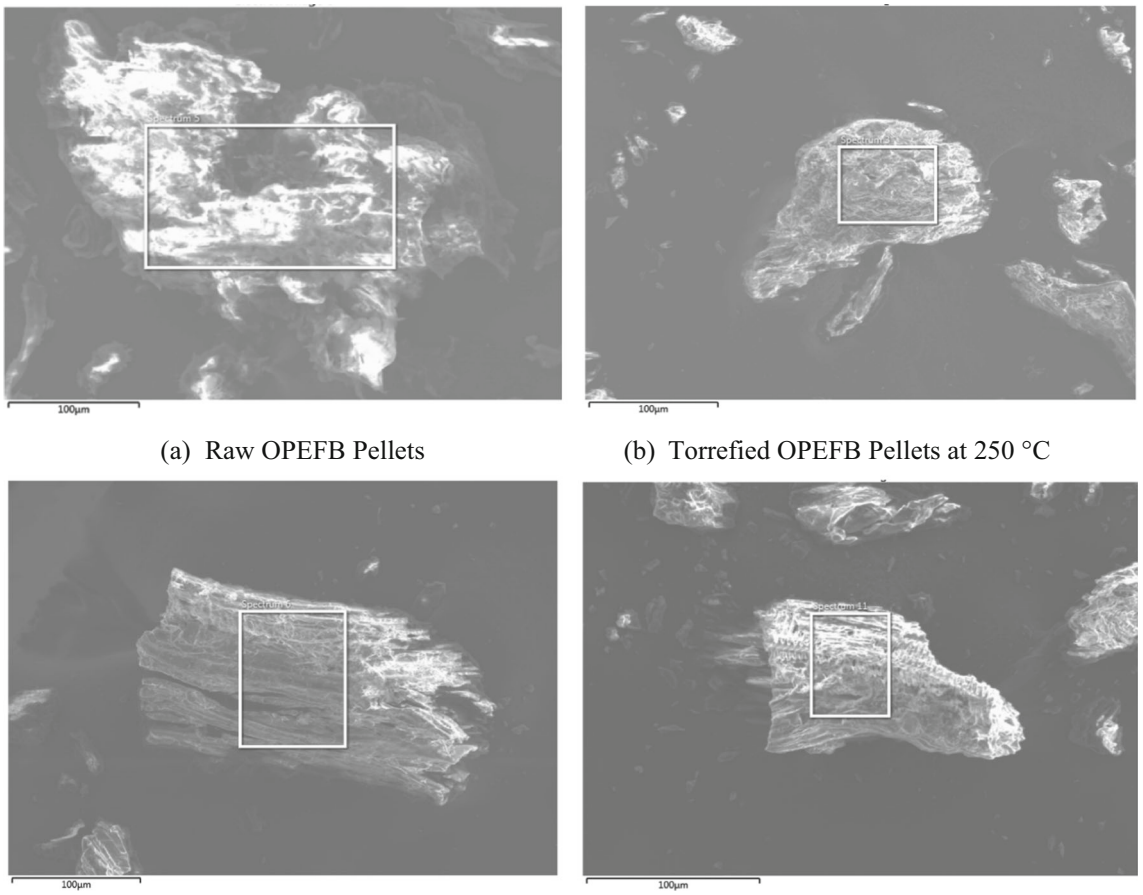

(a) Raw OPEFB Pellets (b) Torrefied OPEFB Pellets at 250 °C

(c) Torrefied OPEFB Pellets at 275 °C (d) Torrefied OPEFB Pellets at 300 °C

Fig. 7 SEM micrographs of raw and CO_2 torrefied OPEFB pellets (a)Raw OPEFB pellets (b)Torrefied OPEFB pellets at 250 °C (c) Torrefied OPEFB pellets at 275 °C (d) Torrefied OPEFB pellets at 300 °C

3.3.4 Hydrophobicity properties

The hydrophobic properties of the CO_2 torrefied OPEFB pellets from 250 to 300 °C for 30 minutes were examined. The results indicate that the torrefied pellets absorbed 63.02, 47.93, and 21.75% water, after torrefaction at 250 °C, 275 °C, and 300 °C, respectively, for 30 minutes. It was also observed that the structure of the torrefied pellets remained intact after the 2-h hydrophobicity tests, whereas the raw pellets totally crumbled due to high water absorption and its poor hydrophobic properties. The improved hydrophobic properties of the torrefied pellets could be attributed to the loss of hydrogen bond linkages between the H and –OH groups that typically facilitate water absorption. This inference is corroborated by the decrease in atomic O/C and H/C ratios of the torrefied OPEFB pellets. The results also indicate that, although the hydrophobicity was improved after torrefaction, the torrefied pellets still absorbed water despite the lower atomic ratios and torrefaction at severe conditions. This observation suggests that other factors such as the microstructure and porosity of torrefied biomass may also play a role in hydrophobicity. The results confirmed that torrefaction significantly reduced the hygroscopicity of the raw OPEFB pellets. Thus, the life span, storage and transportation of the torrefied pellets could be enhanced along with its potential for co-firing or direct combustion as solid biofuels.

3.3.5 Grindability properties

Figure 8 presents the grindability results for the raw and pellets torrefied from 250 to 300 °C for 30 minutes based on the HGI [46]. The initial HGI of 53.66 for the raw OPEFB pellets increased to 76.95, 89.67 and 117.66 after torrefaction at 250, 275 and 300 °C, respectively. This represents changes of 23.29, 36.01 and 64.00 (or by factors of 1.43, 1.67 and 2.19) based on the grindability of the raw pellets.

Typically, the lower the HGI value, the harder it is to grind the material [47]. Therefore, the results demonstrate that the resistance to mechanical degradation (grinding) diminished after torrefaction, which could be due to several factors. Firstly, the improved grindability is typically credited to the degradation or depolymerisation of lignocellulosic components [34, 62]. Secondly, the thermal degradation of holocellulose during torrefaction ruptures the cell wall thereby

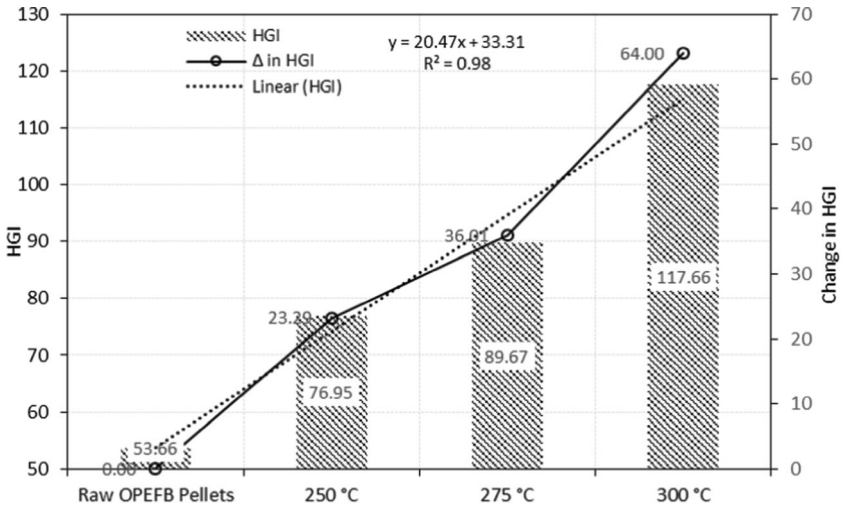

Fig. 8 Grindability of raw and CO_2 torrefied OPEFB pellets

creating pores on the surface of the biomass particles. As a result, the surface area, porosity and brittleness of the biomass particles increase, thereby enhancing its grindability [34, 37]. The drying, devolatilization and decarboxylation reactions that occurred during the CO_2 torrefaction process may also account for the improved grindability as postulated in the literature [48, 63, 64]. To verify this, the moisture and volatile matter of the raw and torrefied OPEFB pellets were examined alongside the HGI, as presented in Fig. 9.

The correlation between the grindability and the physicochemical properties of the raw OPEFB and torrefied pellets is linear under the conditions examined in this study. Therefore, the grindability of the pellets was improved as the MC and VM decreased after torrefaction. The plausible inference is that torrefaction resulted in drying (removal of water) and devolatilization (loss of volatile matter). As a result, the pellets experienced shrinkage due to lower mass yield [41], increased surface porosity and brittleness [27], which reduced resistance to mechanical fractionation during grinding. Secondly, the depolymerisation of cellulose and lignin may also account for the improved grindability after torrefaction [27, 37]. The process of torrefaction thermally degrades the highly branched, rigid and complex polymeric structures of cellulose and lignin of biomasses. Due to depolymerisation, the structural rigidity of the cell wall is significantly deteriorated resulting in the loss of particle cohesiveness and hydrogen bonding [65, 66]. Consequently, the resistance of the torrefied pellets to mechanical disintegration is reduced, thereby enhancing post torrefaction grindability.

3.3.6 Thermal properties

The thermal degradation behaviour and temperature profile characteristics of the raw and OPEFB pellets torrefied from 250 to 300 °C for 30 minutes were examined by TGA. The TG (%) and derivative TG (%/min) plots for the samples are presented in Figs. 10 and 11, respectively.

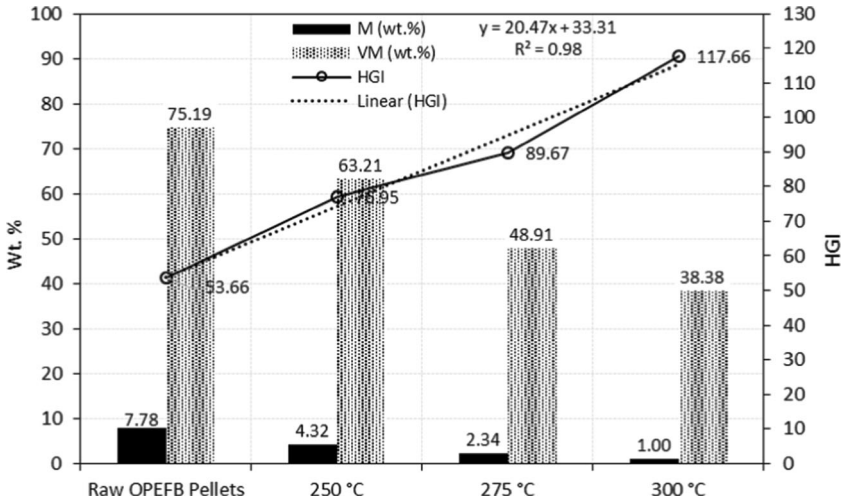

Fig. 9 HGI and properties of raw and CO_2 torrefied OPEFB pellets

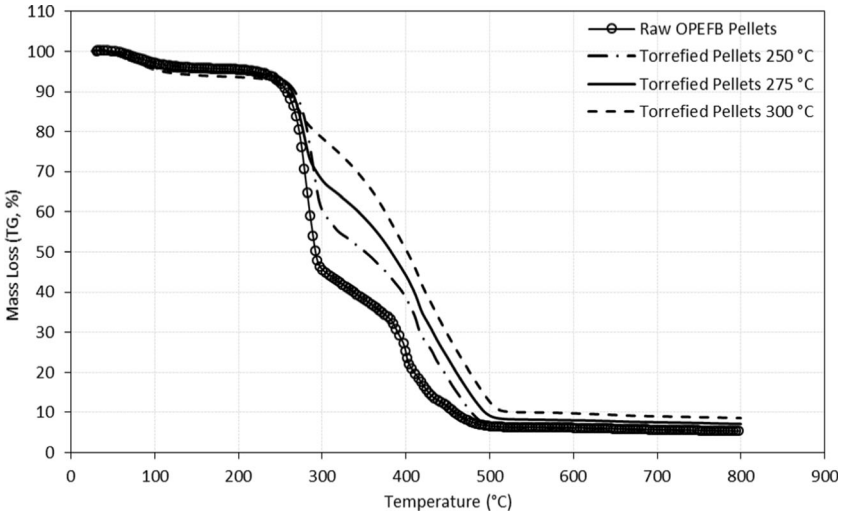

Fig. 10 TG Plots for Raw and CO_2 Torrefied OPEFB pellets

The results demonstrate that the raw and torrefied OPEFB pellets experienced significant mass loss, as evident in downward sloping "double z" or "two-step" curves observed after TGA. The TG plots of the torrefied OPEFB pellets shifted further away from the raw pellets from the left to the right-hand side (RHS) with increasing severity of the torrefaction temperatures. The observed shifts could be ascribed to the thermal lag [67] due to the torrefaction-induced transformations of the proximate fuel properties of the raw pallets after torrefaction. As earlier surmised in Table 5, torrefaction resulted in higher C and FC but lower VM in the torrefied pellets compared with the raw OPEFB pellets. The extent of the TG plot shifts and thermal reactivity of the torrefied OPEFB pellets can be examined from the TPCs presented in Table 6.

The findings indicate that the T_{onset} and T_{offset} temperatures for the raw OPEFB pellets shifted to higher temperatures after torrefaction. The findings also indicate the thermal reactivity of the pellets declined after torrefaction, which could be ascribed to the changes in physicochemical properties (higher C but lower VM content). In particular, the higher T_{onset} values can be explained by the high carbon and fixed carbon but low volatile matter in the torrefied pellets compared with the raw OPEFB pellets (Table 5). Furthermore, the ignitability and reactivity of biomass are influenced by VM and hemicellulose [27], respectively, both of which are devolatilized or thermally degraded during torrefaction. Similar results reported for high-ranked coals and Petcoke were also ascribed to high C and low VM contents [68, 69]. The diminished reactivity of the torrefied pellets is confirmed by the decrease in M_L from 94.90 (raw OPEFB pellets) to 93.04 and 91.56%, while the R_M increased to 6.96 and 8.44% after torrefaction at temperatures of 275 and 300 °C, respectively. This shows the residual masses increased with increasing severity of torrefaction.

The decomposition mechanism and reaction pathway for the raw and torrefied OPEFB pellets were examined from the DTG plots in Fig. 11. The DTG plots are characterised by three major sets of peaks, based on the size, shape and symmetry, which indicate the thermal analysis occurred in four (4) stages.

Stage I, which occurred between 30 and 200 °C, may be ascribed to drying based on the low mass loss (< 10%) for all samples. Stage II occurred between 200 and 325 °C as characterised by a single symmetric peak for each sample, which may be ascribed to devolatilization due to the significant mass loss that occurred at the maxima denoted as T_{peak} I. Typically, the mass loss between 220 and 450 °C is primarily ascribed to cellulose degradation [27, 37]. The mass loss during the TG analysis is likely due to the degradation of residual cellulose and lignin in the torrefied OPEFB pellets. Stage IV could be attributed to the degradation of lignin which occurs over a wide temperature range. In addition, the raw OPEFB pellets showed an additional peak observed from 440 to 500 °C, whereas the torrefied pellets showed minor shoulder peaks from 350 to 450 °C, which are due to the oxidation of char formed from the degradation of hemicellulose, cellulose and lignin during the oxidative TGA process.

The effect of the processes on the TPCs of the raw and torrefied OPEFB pellets are presented in Table 7. The maximum drying peak temperatures decreased from 84.79 °C to the range 66.79–78.91 °C after torrefaction. The decline could be ascribed to the lower moisture content of the torrefied OPEFB pellets compared with the raw pellets. In stage II, the T_{peak} I values initially increased from 282 to 286.72 °C as observed for torrefied OPEFB pellets at 250 °C, but the T_{peak} I decreased to 275.09 and 268.85 °C after torrefaction at 275 and 300 °C for 30 minutes, respectively.

The decline was also characterised by a decline in mass loss rates (M_{LR}) from 31.83%/min for the raw pellets to 27.45, 17.07 and 4.80 %/min for 250, 275 and 300 °C, respectively. These findings indicate the thermal reactivity of the torrefied OPEFB pellets declined significantly in stage II with

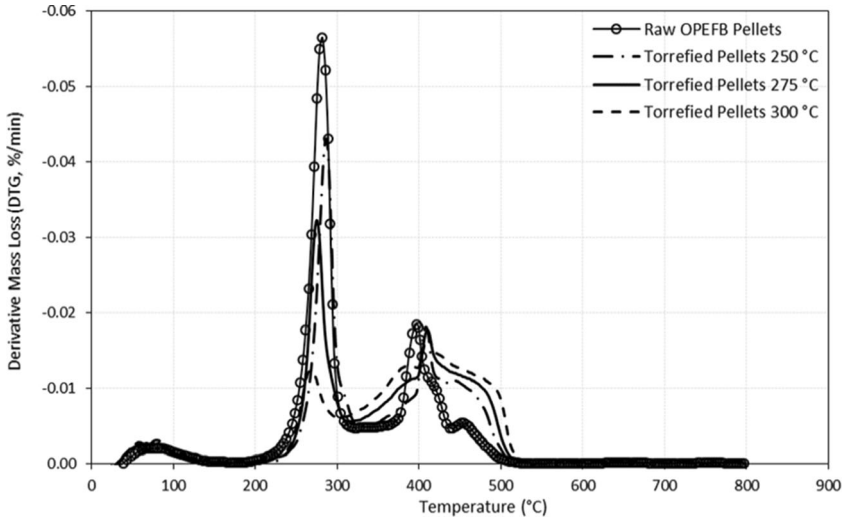

Fig. 11 DTG plots for raw and CO_2 torrefied OPEFB pellets

increasing severity of torrefaction conditions. In stage III, the T_{peak} II values increased from 396.70 °C in the raw OPEFB pellets to 409 °C at 250 °C, 410 °C at 275 °C and 411 °C at 300 °C as observed for the torrefied pellets. Overall, the thermal analysis revealed that the CO_2 torrefaction process severely impacted on the thermal reactivity, degradation behaviour and temperature profiles of the OPEFB pellets.

3.4 Optimization of OPEFB pellets torrefaction

The process of torrefaction is typically aimed at producing high-quality biomass fuels for enhanced energy recovery. Therefore, it is crucial to determine the OOC required to maximize the M_Y during the CO_2 torrefaction of OPEFB pellets through RSM.

3.4.1 Effect of torrefaction parameters on M_Y

Based on the DoE, the CO_2 torrefaction of the OPEFB pellets was performed at temperatures, X_1 = 250, 275 and 300 °C, and time, X_2 = 15, 30 and 60 minutes. The resulting M_Y reported based on the observed and the predicted values are presented in Table 8. The predicted values show excellent agreement with the experimental results (observed dependent variable). This is further confirmed by the low mean square errors and residuals deduced from comparing the data in the Statistica software.

At 95% confidence limit, the mean (weighted) values indicated that temperature (X_1) significantly influenced M_Y compared with time (X_2). The effect of time (X_2) on M_Y was limited to the 15- and 30-minute processes, indicating that torrefaction at 60 minutes did not significantly influence the yield of torrefaction products. Next, the effects of X_1 and X_2 on the mass yield (M_Y) were analysed through the 3D response surface plots presented in Fig. 12.

Based on the response surface plots, a mathematical model representing the effects of X_1 and X_2 on the mass yield (M_Y) was deduced as presented in Eq. 13.

$$Y = 272.55 - 0.5029x_1 - 0.0007x_1^2 - 4.02x_2 + 0.0144x_2^2 + 0.0133x_1x_2 - 0.000012x_1^2x_2 \quad (13)$$

Next, regression analysis was performed to fit the response function and experimental data as required to analyse the model through ANOVA. The analysis was performed to determine the adequacy of the model through the F test and p test. Lastly, the quality of fit was deduced from the coefficients of correlation (R^2 values). The results for the adjusted quadratic model for M_Y of the CO_2 torrefaction of OPEFB pellets are presented in Table 9.

Table 6 Combustion TPCs of raw and CO_2 torrefied pellets

Sample/torrefaction temperature (°C)	Onset (T_{onset}, °C)	Offset (T_{end}, °C)	Mass loss (M_L, %)	Residual mass (R_M, %)
Raw OPEFB pellets	262.01	327.97	94.90	5.10
250	263.09	338.02	94.98	5.02
275	252.88	353.23	93.04	6.96
300	291.89	484.68	91.56	8.44

Table 7 DTG characteristics of raw and CO_2 torrefied OPEFB pellets

Sample/torrefaction temperature (°C)	Stage I	Stage II		Stage III	
	Drying (°C)	T_{peak} I (°C)	MLR (%/min)	T_{peak} II (°C)	MLR (%/min)
Raw OPEFB pellets	84.79	282.00	31.83	396.70	8.74
250	74.50	286.72	27.45	408.58	9.01
275	66.79	275.09	17.07	410.27	7.56
300	78.91	268.85	4.80	411.19	6.30

The findings indicate the independent variables X_1 and X_2 significantly influenced M_Y as evident in the high correlation values (Predicted R^2 = 0.99, Adjusted R^2 = 0.98 and MS Residual of 3.75) observed after the torrefaction process. The difference between the predicted and adjusted R^2 values is less than 0.2, which indicates a good fit or correlation. The ANOVA also revealed that with a *p*-value (< 0.05), all the model terms are significant with the exception of X_1^2 and the interaction terms Temperature (X_1^2) × Time (X_2).

Based on the results, temperature (X_1) is the most significant model term that influenced M_Y during torrefaction, based on its *p* value of (0.00). The most significant interaction model term is Temp (X_1) × Time (X_2) due to its comparatively low *p* value (0.000153) compared with the other terms.

Table 8 Experimental and predicted M_Y for CO_2 torrefaction

SN	Runs	Temperature (°C)	Time (Mins)	Mass yield (M_Y, %)	Predicted values (M_Y, %)
1	R1	250	15	85.32	81.90
2	R2	250	15	83.52	81.90
3	R1	250	30	64.67	69.53
4	R2	250	30	67.00	69.53
5	R1	250	60	65.89	64.17
6	R2	250	60	64.79	64.17
7	R1	275	15	62.66	62.37
8	R2	275	15	61.97	62.37
9	R1	275	30	52.93	52.42
10	R2	275	30	51.70	52.42
11	R1	275	60	49.50	51.92
12	R2	275	60	54.65	51.92
13	R1	300	15	36.93	41.37
14	R2	300	15	40.87	41.37
15	R1	300	30	38.27	33.85
16	R2	300	30	37.03	33.85
17	R1	300	60	35.15	38.21
18	R2	300	60	38.62	38.21

3.4.2 Optimization analysis

The OOC for CO_2 torrefaction was determined by applying the multi-response desirability function in Statistica. Therefore, the predicted response model (*Y*) was aggregated and maximized to determine the optimal conditions for maximizing M_Y from CO_2 torrefaction and deduced from the 3D response surface plots in Fig. 13. Based on the results, the optimal operating conditions (OOC) for maximised M_Y for the CO_2 OPEFB pellet torrefaction are X_1 = 275 °C and X_2 = 35 minutes. Therefore, the predicted mass yield (M_Y), mass loss (M_L) and higher heating value (HHV) for torrefied pellets at the deduced OOC are 50.54%, 49.46% and 24.47 MJ/kg, respectively. In comparison, Chin et al. [40] reported the optimal conditions of 230 °C and 40 minutes for maximized mass yield and HHV of 24.30 MJ/kg from the torrefaction of pulverised OPEFB. The results for OPEFB pellets reported in this study are considered in fairly good agreement with their work.

The RSM optimization results were subsequently validated by performing confirmatory CO_2 torrefaction experiments at the OOCs: temperature X_1 = 275 °C and residence time X_2 = 35 minutes. The confirmatory tests indicated that the CO_2 torrefaction of the OPEFB pellets at the OOCs yielded the mass yield (M_Y) of 52.55%, which corresponds to mass loss (M_L) of 47.46% and HHV of 24.28 MJ/kg. The results showed the M_Y, M_L, and HHV from the confirmatory tests are in excellent agreement with the model prediction in RSM.

4 Conclusions

The torrefaction of oil palm empty fruit bunch pellets was examined under carbon dioxide (CO_2) gas followed by comprehensive analysis of the yield, distribution and characteristics of the M_Y, L_Y and G_Y products. Lastly, optimisation through RSM was performed to determine the OOC for maximum M_Y. The findings indicated that temperature and time significantly influenced the yield and distribution of the CO_2 torrefaction products. It was observed that whereas the M_Y

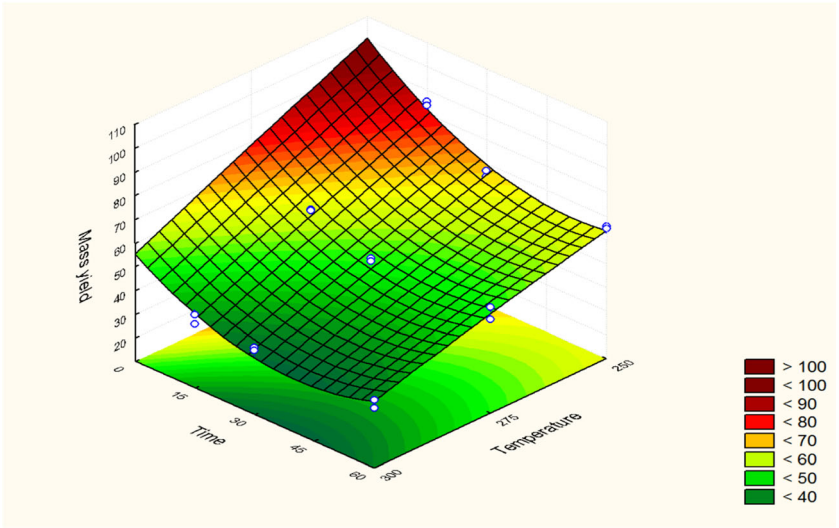

Fig. 12 3D surface plots of mass yield (M_Y, %) for CO_2 torrefaction

Table 9 ANOVA results for the M_Y model

Torrefaction variables	Sum of squares (SS)	Degrees of freedom (df)	Mean square (MS)	*F* value	*p* value
Temperature (X_1)	3228.10	1.00	3228.10	860.92	0.000000
Temperature (X_1^2)	2.19	1.00	2.19	0.58	0.464096
Time (X_2)	327.29	1.00	327.29	87.29	0.000006
Time (X_2^2)	161.13	1.00	161.13	42.97	0.000105
Temp (X_1) × Time (X_2)	145.61	1.00	145.61	38.83	0.000153
Temp (X_1) × Time (X_2^2)	87.20	1.00	87.20	23.26	0.000944
Temp (X_1^2) × Time (X_2)	0.06	1.00	0.06	0.02	0.899687
Error	33.75	9.00	3.75		
Total SS	4128.64	17.00			

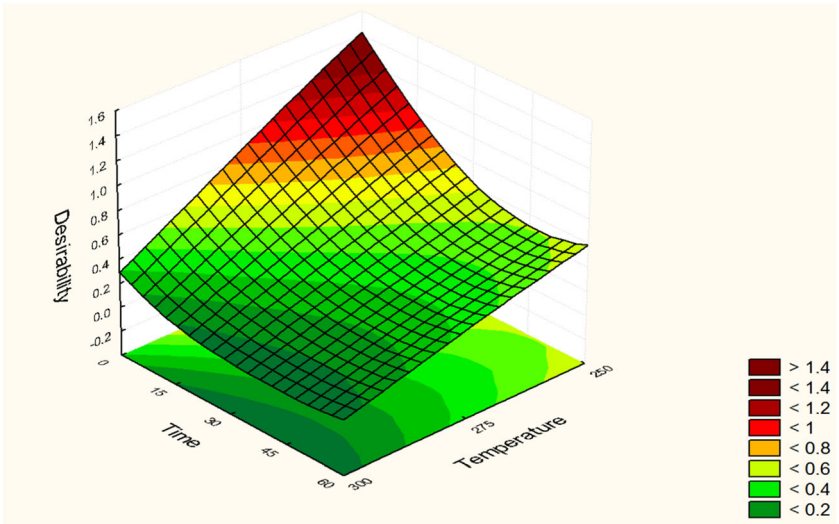

Fig. 13 Desirability of 3D plots for optimal CO_2 torrefaction

and E_Y decreased, the L_Y and G_Y increased with increasing severity of the selected torrefaction conditions. Similarly, the D_E, HHV and S_F were enhanced after torrefaction. The torrefied pellets exhibited significant improvements in their physicochemical, microstructure, grindability and hydrophobic properties compared with the raw OPEFB pellets. The thermal degradation and temperature profile characteristics under oxidative conditions were significantly transformed compared with the raw pellets. The liquid torrefaction products revealed acidic and light brown to dark products with pungent odours comprised largely of water and organic fractions. The RSM optimisation deduced the temperature X_1 = 275 °C and residence time X_2 = 35 minutes as the OOC for the CO_2 torrefaction of OPEFB pellets. In general, the findings of the study revealed that CO_2 torrefaction is a practical technique for sustainable energy recovery from OPEFB pellets.

Acknowledgements The support of the Centre of Hydrogen Energy and the Institute of Future Energy all at the Universiti Teknologi Malaysia (UTM) Skudai Campus in Johor are all gratefully acknowledged. The contributions of the University Industry Research Laboratory (UIRL) is also worthy of thanks for the support during this project.

References

1. Kushairi A, Ong-Abdullah M, Nambiappan B, Hishamuddin E, Bidin MNIZ, Ghazali R, Subramaniam V, Sundram S, Parveez GKA (2019) Oil Palm Economic Performance in Malaysia and R&D Progress in 2018. J Oil Palm Res 31(2):165–194
2. Ganapathy B, Yahya A, Ibrahim N (2019) Bioremediation of palm oil mill effluent (POME) using indigenous Meyerozyma guilliermondii. Environ Sci Pollut Res 26(11):11113–11125
3. Nambiappan B, Ismail A, Hashim N, Ismail N, Nazrima S, Idris NAN, Omar N, Saleh K, Hassan NAM, Kushairi A (2018) Malaysia: 100 years of resilient palm oil economic performance. J Oil Palm Res 30(1):13–25
4. Taufiq-Yap Y, Farabi MA, Syazwani O, Ibrahim ML, Marliza T (2020) Sustainable Production of Bioenergy. In: Ashwani KG, Ashoke D, Suresh KA, Abhijit K, Akshai R (eds) Innovations in sustainable energy and cleaner environment. Springer, Berlin, pp 541–561
5. MPOB (2019) Overview of the Malaysian oil palm industry 2018. Palm Oil Statistics, Malaysian Palm Oil Board (MPOB), Kuala Lumpur
6. AIM (2013) National Biomass Strategy 2020. New wealth creation for Malaysia's palm oil industry, vol 2.0, 2nd edn. Agensi Inovasi Malaysia (AIM), Kuala Lumpur
7. Cazzolla Gatti R, Liang J, Velichevskaya A, Zhou M (2019) Sustainable palm oil may not be so sustainable. Sci Total Environ 652:48–51. https://doi.org/10.1016/j.scitotenv.2018.10.222
8. Loh SK (2017) The potential of the Malaysian oil palm biomass as a renewable energy source. Energy Convers Manag 141:285–298
9. Mahlia TMI, Ismail N, Hossain N, Silitonga AS, Shamsuddin AH (2019) Palm oil and its wastes as bioenergy sources: a comprehensive review. Environ Sci Pollut Res 26, 14849–14866. https://doi.org/10.1007/s11356-019-04563-x
10. Idris J, Shirai Y, Andou Y, Ali AAM, Othman MR, Ibrahim I, Hassan MA (2015) Self-sustained carbonization of oil palm biomass produced an acceptable heating value charcoal with low gaseous emission. J Clean Prod 89:257–261
11. Krishnan Y, Bong CPC, Azman NF, Zakaria Z, Abdullah N, Ho CS, Lee CT, Hansen SB, Hara H (2017) Co-composting of palm empty fruit bunch and palm oil mill effluent: microbial diversity and potential mitigation of greenhouse gas emission. J Clean Prod 146:94–100
12. Abdulrazik A, Elsholkami M, Elkamel A, Simon L (2017) Multi-products productions from Malaysian oil palm empty fruit bunch (EFB): Analyzing economic potentials from the optimal biomass supply chain. J Clean Prod 168:131–148. https://doi.org/10.1016/j.jclepro.2017.08.088
13. Shanmugarajah B, Chew IM, Mubarak NM, Choong TS, Yoo C, Tan K (2019) Valorization of palm oil agro-waste into cellulose biosorbents for highly effective textile effluent remediation. J Clean Prod 210:697–709. https://doi.org/10.1016/j.jclepro.2018.10.342
14. Abdullah N, Sulaiman F (2013) The oil palm wastes in Malaysia. In: Biomass Now-Sustainable Growth and Use, vol 1. InTech Open Publishers, pp 75-93
15. Sumathi S, Chai S, Mohamed A (2008) Utilization of oil palm as a source of renewable energy in Malaysia. Renew Sust Energ Rev 12(9):2404–2421
16. Lee KT, Ofori-Boateng C (2013) Utilisation of Palm Oil Wastes for Biofuel and Other Value-Added Bio-Products: A Holistic Approach to Sustainable Waste Management for the Palm Oil Industry. In: Pogaku R., Sarbatly R. (Eds) Advances in Biofuels. pp 53-87, Springer, Boston, MA, USA. https://doi.org/10.1007/978-1-4614-6249-1_5
17. Mohammed MAA, Salmiaton A, Wan Azlina WAKG, Mohammad Amran MS, Fakhru'l-Razi A (2011) Air gasification of empty fruit bunch for hydrogen-rich gas production in a fluidized-bed reactor. Energy Convers Manag 52(2):1555–1561. https://doi.org/10.1016/j.enconman.2010.10.023
18. Lahijani P, Zainal Z (2014) Fluidized bed gasification of palm empty fruit bunch using various bed materials. Energy Sources A: Recov Util Environ Effects 36(22):2502–2510
19. Sivasangar S, Zainal Z, Salmiaton A, Taufiq-Yap YH (2015) Supercritical water gasification of empty fruit bunches from oil palm for hydrogen production. Fuel 143:563–569. https://doi.org/10.1016/j.fuel.2014.11.073
20. Olugbade T, Ojo O, Mohammed T (2019) Influence of Binders on combustion properties of biomass briquettes: a recent review. BioEnergy Res 12(2):241–259
21. Zaini IN, Novianti S, Nurdiawati A, Irhamna AR, Aziz M, Yoshikawa K (2017) Investigation of the physical characteristics of washed hydrochar pellets made from empty fruit bunch. Fuel Process Technol 160:109–120. https://doi.org/10.1016/j.fuproc.2017.02.020
22. Ruksathamcharoen S, Chuenyam T, Stratong-on P, Hosoda H, Ding L, Yoshikawa K (2019) Effects of hydrothermal treatment and pelletizing temperature on the mechanical properties of empty fruit bunch pellets. Appl Energy 251:113385
23. Salema AA, Ani FN (2012) Pyrolysis of oil palm empty fruit bunch biomass pellets using multimode microwave irradiation. Bioresour Technol 125:102–107
24. Lam PS, Lam PY, Sokhansanj S, Lim CJ, Bi XT, Stephen JD, Pribowo A, Mabee WE (2015) Steam explosion of oil palm residues for the production of durable pellets. Appl Energy 141:160–166
25. Erlich C, Fransson TH (2011) Downdraft gasification of pellets made of wood, palm-oil residues respective bagasse:

Experimental study. Appl Energy 88(3):899–908. https://doi.org/10.1016/j.apenergy.2010.08.028
26. Sukiran MA, Abnisa F, Daud WMAW, Bakar NA, Loh SK (2017) A review of torrefaction of oil palm solid wastes for biofuel production. Energy Convers Manag 149:101–120
27. Basu P (2018) Biomass gasification, pyrolysis and torrefaction: practical design and theory, vol 2. Academic Press (Elsevier), London
28. Uemura Y, Omar WN, Tsutsui T, Yusup SB (2011) Torrefaction of oil palm wastes. Fuel 90(8):2585–2591
29. Faizal HM, Shamsuddin HS, Heiree MHM, Hanaffi MFMA, Rahman MRA, Rahman MM, Latiff ZA (2018) Torrefaction of densified mesocarp fibre and palm kernel shell.Renewable Energy, 122, 419-428. https://doi.org/10.1016/j.renene.2018.01.118
30. Sellappah V, Uemura Y, Hassan S, Sulaiman MH, Lam MK (2016) Torrefaction of empty fruit bunch in the presence of combustion gas. Proc Eng 148:750–757. https://doi.org/10.1016/j.proeng.2016.06.608
31. Uemura Y, Sellappah V, Trinh TH, Hassan S, Tanoue K-i (2017) Torrefaction of empty fruit bunches under biomass combustion gas atmosphere. Bioresour Technol 243:107–117
32. Uemura Y, Omar W, Othman NA, Yusup S, Tsutsui T (2013) Torrefaction of oil palm EFB in the presence of oxygen. Fuel 103:156–160
33. Uemura Y, Saadon S, Osman N, Mansor N, Tanoue K-i (2015) Torrefaction of oil palm kernel shell in the presence of oxygen and carbon dioxide. Fuel 144:171–179
34. Thanapal SS, Chen W, Annamalai K, Carlin N, Ansley RJ, Ranjan D (2014) Carbon dioxide torrefaction of woody biomass. Energy Fuel 28(2):1147–1157
35. Rasid RA, Yusoff MHM (2017) The potential of CO2 torrefaction as biomass Pre-treatment method. Indian J Sci Technol 10:1–5
36. Asadullah M, Adi AM, Suhada N, Malek NH, Saringat MI, Azdarpour A (2014) Optimization of palm kernel shell torrefaction to produce energy densified bio-coal. Energy Convers Manag 88:1086–1093. https://doi.org/10.1016/j.enconman.2014.04.071
37. Chen WH (2015) Torrefaction. In: Pandey A, Negi S, Binod P, Larroche C (eds) Pretreatment of biomass: processes and technologies, vol 1. Elsevier BV, Oxford, p 261
38. Peng J, Bi H, Sokhansanj S, Lim J (2012) A study of particle size effect on biomass torrefaction and densification. Energy Fuel 26(6):3826–3839
39. Gan YY, Ong HC, Ling TC, Chen W-H, Chong CT (2019) Torrefaction of de-oiled Jatropha seed kernel biomass for solid fuel production. Energy 170:367–374
40. Chin K, H'ng P, Go W, Wong W, Lim T, Maminski M, Paridah M, Luqman A (2013) Optimization of torrefaction conditions for high energy density solid biofuel from oil palm biomass and fast growing species available in Malaysia. Ind Crop Prod 49:768–774
41. Erlich C (2009) Comparative study of residue pellets from cane sugar and palm-oil industries with commercial wood pellets, applied in downdraft gasification. KTH Royal Institute of Technology, Stockholm
42. Brunerová A, Müller M, Šleger V, Ambarita H, Valášek P (2018) Bio-pellet fuel from oil palm empty fruit bunches (EFB): Using European standards for quality testing. Sustainability 10(12):4443
43. Na B-I, Ahn B-J, Lee J-W (2015) Changes in chemical and physical properties of yellow poplar (Liriodendron tulipifera) during torrefaction. Wood Sci Technol 49(2):257–272
44. Rajkovich S, Enders A, Hanley K, Hyland C, Zimmerman AR, Lehmann J (2012) Corn growth and nitrogen nutrition after additions of biochars with varying properties to a temperate soil. Biol Fertil Soils 48(3):271–284
45. Pimchuai A, Dutta A, Basu P (2010) Torrefaction of agriculture residue to enhance combustible properties. Energy Fuel 24(9):4638–4645
46. Ibrahim RH, Darvell LI, Jones JM, Williams A (2013) Physicochemical characterisation of torrefied biomass. J Anal Appl Pyrolysis 103:21–30
47. Shang L, Ahrenfeldt J, Holm JK, Sanadi AR, Barsberg S, Thomsen T, Stelte W, Henriksen UB (2012) Changes of chemical and mechanical behaviour of torrefied wheat straw. Biomass Bioenergy 40:63–70
48. Ohliger A, Förster M, Kneer R (2013) Torrefaction of beechwood: a parametric study including heat of reaction and grindability. Fuel 104:607–613
49. Chen W-H, Liu S-H, Juang T-T, Tsai C-M, Zhuang Y-Q (2015) Characterization of solid and liquid products from bamboo torrefaction. Appl Energy 160:829–835
50. Bridgwater AV (2012) Upgrading biomass fast pyrolysis liquids. Environ Prog Sustain Energy 31(2):261–268
51. Zhao L, Zheng W, Cao X (2014) Distribution and evolution of organic matter phases during biochar formation and their importance in carbon loss and pore structure. Chem Eng J 250:240–247. https://doi.org/10.1016/j.cej.2014.04.053
52. Pandey A (2008) Handbook of plant-based biofuels. Engineering & Technology, Environment & Agriculture. CRC Press, Boca Raton
53. Oasmaa A, Elliott DC, Korhonen J (2010) Acidity of biomass fast pyrolysis bio-oils. Energy Fuel 24(12):6548–6554
54. Kim D, Lee K, Park KY (2014) Hydrothermal carbonization of anaerobically digested sludge for solid fuel production and energy recovery. Fuel 130:120–125
55. Poudel J, Ohm TI, Gu JH, Shin MC, Oh SC (2017) Comparative study of torrefaction of empty fruit bunches and palm kernel shell. J Mater Cycles Waste Manag 19(2):917–927. https://doi.org/10.1007/s10163-016-0492-1
56. Mohammed MAA, Salmiaton A, Wan Azlina WAKG, Mohamad Amran MS (2012) Gasification of oil palm empty fruit bunches: a characterization and kinetic study. Bioresour Technol 110:628–636. https://doi.org/10.1016/j.biortech.2012.01.056
57. Lu T, Li K-Z, Zhang R, Bi J-C (2015) Addition of ash to prevent agglomeration during catalytic coal gasification in a pressurized fluidized bed. Fuel Process Technol 134:414–423
58. Patrick DO, Yusup S, Osman NB, Zabiri H, Uemura Y, Shahbaz M (2020) Thermogravimetric kinetics of catalytic and non-catalytic pyrolytic conversion of palm kernel shell with acid-treated coal bottom ash. BioEnergy Res 1(1):1–11
59. Chen W-H, Lu K-M, Lee W-J, Liu S-H, Lin T-C (2014) Non-oxidative and oxidative torrefaction characterization and SEM observations of fibrous and ligneous biomass. Appl Energy 114(1):104–113
60. Nyakuma BB, Wong S, Oladokun O (2019) Non-oxidative thermal decomposition of oil palm empty fruit bunch pellets: fuel characterisation, thermogravimetric, kinetic, and thermodynamic analyses. Biomass Convers Biorefine. https://doi.org/10.1007/s13399-13019-00568-13391
61. Kristensen JB, Thygesen LG, Felby C, Jørgensen H, Elder T (2008) Cell-wall structural changes in wheat straw pretreated for bioethanol production. Biotechnol Biofuels 1(1):1–9
62. Iroba KL, Baik O-D, Tabil LG (2017) Torrefaction of biomass from municipal solid waste fractions I: temperature profiles, moisture content, energy consumption, mass yield, and thermochemical properties. Biomass Bioenergy 105:320–330. https://doi.org/10.1016/j.biombioe.2017.07.009

63. Phanphanich M, Mani S (2011) Impact of torrefaction on the grindability and fuel characteristics of forest biomass. Bioresour Technol 102(2):1246–1253
64. Arias B, Pevida C, Fermoso J, Plaza MG, Rubiera F, Pis J (2008) Influence of torrefaction on the grindability and reactivity of woody biomass. Fuel Process Technol 89(2):169–175
65. Wang G, Luo Y, Deng J, Kuang J, Zhang Y (2011) Pretreatment of biomass by torrefaction. Chin Sci Bull 56(14):1442–1448
66. Cao L, Yuan X, Li H, Li C, Xiao Z, Jiang L, Huang B, Xiao Z, Chen X, Wang H (2015) Complementary effects of torrefaction and co-pelletization: Energy consumption and characteristics of pellets. Bioresour Technol 185:254–262
67. Slopiecka K, Bartocci P, Fantozzi F (2012) Thermogravimetric analysis and kinetic study of poplar wood pyrolysis. Appl Energy 97:491–497. https://doi.org/10.1016/j.apenergy.2011.12.056
68. Zhan X, Jia J, Zhou Z, Wang F (2011) Influence of blending methods on the co-gasification reactivity of petroleum coke and lignite. Energy Convers Manag 52(4):1810–1814
69. Nemanova V, Abedini A, Liliedahl T, Engvall K (2014) Co-gasification of petroleum coke and biomass. Fuel 117:870–875